Applied Catalysis B: Environmental 165 (2015) 715–722

Contents lists available at ScienceDirect

Applied Catalysis B: Environmental

journal homepage: www.elsevier.com/locate/apcatb

C-doped hollow TiO_2 spheres: in situ synthesis, controlled shell thickness, and superior visible-light photocatalytic activity

Ying Zhang[a], Zhiyuan Zhao[a], Juanrong Chen[b], Li Cheng[a], Jun Chang[a], Weichen Sheng[a], Changyuan Hu[c], Shunsheng Cao[a,*]

[a] School of Chemistry and Chemical Engineering, Jiangsu University, Zhenjiang 212013, China
[b] School of Environment and Safety Engineering, Jiangsu University, Zhenjiang 212013, China
[c] Jiangxi Key Laboratory of Surface Engineering, Jiangxi Science and Technology Normal University, Nanchang 330013, P. R. China

ARTICLE INFO

Article history:
Received 11 August 2014
Received in revised form 17 October 2014
Accepted 22 October 2014
Available online 1 November 2014

Keywords:
In situ synthesis
C-doping
Hollow TiO_2
Photocatalysis
Visible-light photocatalytic activity.

ABSTRACT

The persistent efforts have been paid to shift the ultraviolet of titania to visible-light-driven photocatalysis. In this work, we explored a facile, cost-effective method to *in situ* create C-doped hollow TiO_2 spheres. This method involved the preparation of monodisperse cationic polystyrene spheres (CPS), sequential deposition of TiO_2 precursor via template-directed self-assembly, and the removal of CPS template by calcination at 450 °C. The structure and properties of hollow TiO_2 catalysts were characterized by N_2 desorption–adsorption, X-ray diffraction (XRD), UV–vis spectroscopy, and X-ray photoelectron spectroscopy (XPS). Results confirmed the carbon doping in the as-prepared hollow TiO_2 lattice. When C-doped hollow TiO_2 spheres were used as photocatalysts for the degradation of Rhodamine B under visible-light irradiation, the as-synthesized hollow anatase exhibited a superior photocatalytic activity than the commercial P25 and many TiO_2-based photocatalysts reported in literature, significantly broadening its potential for many practical applications.

1. Introduction

Extending the TiO_2 photoresponse spectrum to the visible region has caught increasing attention of a number of investigators because of its intrinsic drawbacks, such as wide band gap and considerable recombination of the photo-generated electron–hole pairs, severely limiting the activity only under ultraviolet (UV) light irradiation and its efficiency [1,2]. Effective strategies to tackle this challenge can tailor by incorporation of additional components in TiO_2 structure including metallic and non-metallic doping [3,4]. However, metal doping of TiO_2 often suffers from poor thermal stability, photo-corrosion, and is more prone to serve as recombination centers due to the dopants' localized d-states deep in the band gap of TiO_2 [5,6]. By contrast, non-metal (C, B, F, N, etc.) doping is far more successful than metal doping in shifting the ultraviolet to the visible light range[5]. In particular, carbon doping exhibits considerable potential advantages over other types of non-metal doping, which may be responsible for the following reasons [6,7]: Firstly, carbon presents metallic conductivity as one of the many possible electronic materials [8]; Secondly, carbon has a large electron-storage capacity and can accept the photon-excited electrons to enhance the separation of photo-generated carries [9,10]; Thirdly, carbon holds a wide range of visible light absorption at a wavelength of 400–800 nm, thus facilitating charge transfer from the bulk of the TiO_2 to the surface region where the desired oxidation reaction takes place [11,12]. More importantly, in the process of carbon doping, carbon element is always indicated permeating to the lattice of TiO_2 substituting a lattice O atom and forms O–Ti–C bond, which produces a hybrid orbital just above the valence band of TiO_2 and bestows an enhanced visible-light absorbance [5,7].

A number of effective strategies have been developed to engineer C/TiO_2 nanoparticles including sol–gel method with carbon precursors, direct burning of titanium metal in natural gas flame, annealing TiO_2 under CO gas flow at high temperature, and thermal oxidation of TiC [6,11,13,14]. For example, Lu et al. [13] prepared a carbon surface-modified C/TiO_2 photocatalyst by thermal treatment of phenylphosphonic acid/TiO_2, and Sampath et al. [15] introduced a simple protocol for the preparation of one-dimensional (1D) oxidized titanium carbide nanowires using thermal oxidation of TiC. However, above-mentioned methods to incorporate carbon element to TiO_2 have limitations because addition of external carbon precursors is required and aggregation

* Corresponding author.
E-mail addresses: sscaochem@hotmail.com, sscao@ujs.edu.cn (S. Cao).

http://dx.doi.org/10.1016/j.apcatb.2014.10.063
0926-3373/

of carbon species commonly arises [16]. Therefore, novel designs and strategies for creating functional C/TiO_2 materials with highly visible-light efficiency are urged.

Hollow TiO_2 materials appear to be more attractive than solid TiO_2 nanoparticles due to their increased surface area and multiple interparticle scattering [12,17]. Controlling over the morphology and particle size of hollow TiO_2 has been pursuing object because it is a crucial parameter determining the photocatalytic performances of hollow TiO_2 spheres [18]. However, the current methods of TiO_2 hollow materials represent one of the main challenges that impede the development of industrial-scale photocatalytic process. Generally, such methods can be classified into two main strategies: template-free and template-directed methods. The former allows one-pot and large-scale synthesis of hollow TiO_2 particles with tunable morphology and structure via physical phenomenon [19]. However, a major drawback of this technique is the concomitant production of a large fraction of dispersed particles, and the spherical products are usually ill-shaped and fragile [20]. In contrast, the latter is a promising way to overcome the disadvantages because this technique can effectively confine the formation of titania shell based on the preformed templates and allow the construction of hollow TiO_2 particles with well-controlled dimension, interior-cavity size, and tunable shell thickness [21,22]. However, maintaining the porosity and surface area during amorphous-to-crystalline transition is a major challenge in the synthesis of the semiconductor TiO_2 photocatalyst.

Inspired by the above-described considerations, we devise a facile, cost-effective strategy for the construction of the C-doped hollow TiO_2 spheres with tunable architectures. The C-doped TiO_2 hollow spheres not only offer an advantage over the existed methods because they are *in situ* formed by directly carbonizing cationic polystyrene templates (CPS) without additional carbon precursors, but also hold a narrow pore size distribution and controlled shell thickness. Unexpectedly, the C-doped hollow TiO_2 spheres perfectly retain their nanostructures during amorphous-to-crystalline transition and manifest a superior visible-light photocatalytic activity far over the commercial P25 and many TiO_2-based photocatalysts reported in literature [23–27], significantly broadening their potential for many practical applications [23–28].

2. Experimental

2.1. Materials

Unless otherwise noted, chemicals and drugs were available from Sigma-Aldrich Company Ltd and used as-received without further purification. Styrene, $K_2S_2O_8$, and absolute ethanol were the products of the Sinopharm Chemical Reagent Co., Ltd (China) and were used as-received except styrene (St), which was purified with 5 wt% NaOH solution prior to use. Water for the reaction and analysis was collected from the Direct-Q UV System (Millipore).

2.2. Cationic polystyrene spheres

The monodisperse cationic polystyrene spheres (CPS) were prepared via emulsifier-free polymerization according to our previous works [29,30]: $K_2S_2O_8$, H_2O, and styrene were placed into a 100 mL four-necked flask equipped with a mechanical stirrer, an N_2 inlet, a Graham condenser, and a heating mantle. After flushing the system with nitrogen gas for 20 min, the polymerization was conducted at 70 °C for 4 h with a stirring rate of 400 rpm, followed by the continuous addition of DMC (2-(methacryloyloxy)ethyltrimethylammonium chloride). The resulting solid was filtered and washed for three times with warm deionized water.

2.3. The synthesis of C-doped hollow TiO_2 spheres

Cationic polystyrene spheres (CPS) were dispersed into absolute ethanol at ice-water bath, followed by the slow addition of tetrabutyl orthotitanate (TBT) dissolved with absolute ethanol. After completing these, the reactive medium was further kept for 24 h to allow a saturated adsorption of TBT on the surface of CPS, and then suitable ammonia was added into this system to allow the sol–gel process to occur, forming CPS/TiO_2 core/shell particles. The solid product was filtered and washed repeatedly with deionized water, dried, and then calcined at 450 °C. In addition, the shell thickness of hollow TiO_2 spheres was determined from the SEM image of broken particles and the cross-section TEM images of the sample via software of digital micrograph.

2.4. Characterization of C-doped hollow TiO_2 spheres

The internal and external morphologies of these prepared TiO_2 microspheres were measured using a transmission electron microscope (TEM) and a scanning electron microscope (SEM), respectively. The particle size distributions of the hollow TiO_2 spheres were determined by means of dynamic light scattering (DLS), performing at 25 °C at a scattering angle of 90° using a goniometer equipped with a self-rotation unit and a He–Ne laser (Mastersizer-X). In addition, thermogravimetric analysis (TGA), X-ray diffraction (XRD), elemental analysis (EA), X-ray photoelectron spectroscopy (XPS), and UV–vis spectrometry were used to monitor structure, morphology, and components of C-doped hollow TiO_2 spheres.

2.5. Photocatalytic activity measurement

The photocatalytic activity of catalysts was evaluated by the degradation of Rhodamine B (RhB) in an aqueous solution containing 0.01 mM RhB as initial concentrations and 1 g/L catalysts in 50 mL glass vessels by referring previous publications [23,26]. The visible-light source used ozone-free Xe arc lamp (XHA350 W, 350 W) attached with UV cut filter (FSQ-GC 400). The suspension was stirred vigorously for 60 min in the dark to establish adsorption–desorption equilibrium of RhB, and then was irradiated under visible light. Samples were withdrawn periodically from the reactor, then centrifuged, and analyzed by recording variations in the absorption in the UV–vis spectra of RhB (λ = 553 nm) [25,28]. In addition, the degradation (complete mineralization) of Rhodamine B was monitored by using total organic carbon (TOC) analysis.

3. Results and discussion

3.1. The preparation of C-doped hollow TiO_2 spheres

The C-doped hollow TiO_2 spheres were *in situ* synthesized in three steps by using a template-guided self-assembly, as demonstrated in Scheme 1. Firstly, monodisperse cationic polystyrene spheres (CPS) were prepared via emulsion-free polymerization. In the subsequent coating process, CPS template was dispersed into absolute ethanol at ice-water bath, followed by the slow addition of tetrabutyl orthotitanate (TBT) dissolved with absolute ethanol. After these, suitable ammonia was added into the system to allow the sol–gel process to occur, forming CPS/TiO_2 core/shell particles. Finally, CPS was removed by calcination at 450 °C and simultaneously accompanied with a phase transition from amorphous to crystalline, *in situ* producing C-doped hollow anatase TiO_2 spheres. In comparison with the near-perfect spherical CPS templates (Fig. S1), the TiO_2-deposited CPS (CPS/TiO_2 particles) exhibits a rough surface and less than perfect spherical shape with the increased average diameter, which is clearly ascribed to the coating

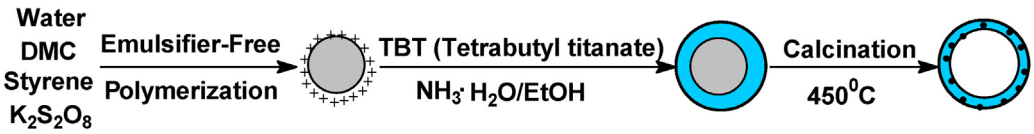

Scheme 1. In situ synthesis of the C-doped hollow TiO_2 spheres.

of a TiO_2 layer on the spherical CPS core (Fig. S2). The formation mechanism of CPS/TiO_2 core/shell composites is regarded to be caused by electrostatic deposition because the isoelectric point of TiO_2 nanoparticles is reported to be 5–6 [31], indicating that CPS core is critical for the uniform deposition of titania precursor on the surface of templates and ultimately determine the size and shape of the final products [30,32].

As showed in Fig. 1a, a noticeable difference in the gray scale of the TEM image of TiO_2 hollow spheres (due to the difference in electron density) confirms that the produced particles are hollow and porous in nature [24,33]. In particular, the uniform shells imply that synthesized hollow TiO_2 spheres have a good thermal stability because they are enough strong to survive after calcination at 450 °C, maintaining their porosity and morphology during the process of TiO_2 phase transition from amorphous to crystalline. TGA curve shows that CPS template can be completely removed by calcination at 450 °C (Fig. S3a). Another representative SEM image in Fig. 1b indicates that they have a highly ordered and well-defined morphology, as fairly agrees with results determined by dynamic light scattering (Fig. S3b). Several broken microspheres further reveal the hollow nature of these TiO_2 [34]. All the experimental results and discussion suggest that the ordered C-doped hollow TiO_2 spheres have been successfully developed by using CPS as templates.

3.2. Preparation of C-doped hollow TiO_2 spheres with controlled shell thickness

Shell thickness of hollow TiO_2 spheres has been shown to dictate the mechanical strength and the permeability of the shell [35,36]. In this work, the thickness of C-doped hollow TiO_2 spheres can be adjusted only through changing the addition amount of the titania precursor. Fig. 2 shows the SEM and TEM images of the C-doped hollow TiO_2 spheres produced with different amount of TBT added. When the addition amount of TBT is only 1 g, a number of broken spheres are observed, suggesting that the amount of TBT is not enough to completely surround the CPS templates (Fig. S4). When the addition amount of TBT is 2 g, the dark single curve at the edge of each particle is consistent with each hollow sphere having one uniform shell thickness of ~20 nm by measuring the dark ring on the perimeter of the hollow spheres. When the amount of TBT is increased to 3 g, a higher shell thickness (~29 nm) of hollow TiO_2 spheres is obtained. When the amount of TBT is further increased to 4 g, the thickness increases to about 45 nm. When the amount of TBT is 5 g, the shell thickness approaches 59 nm. The SEM and TEM images highlight the fact that hollow TiO_2 spheres are well defined and demonstrate homogeneous shell thickness. On the other hand, if the shell thickness of hollow TiO_2 spheres was able to be adjusted simply by changing the addition amount of TBT precursors, their BET surface area would also be changed accordingly. To confirm the hypothesis, we have measured the dependence of the BET surface area on the addition amount of TBT. Fig. 3 demonstrates that the BET surface area is 39.446, 50.270, 17.623, and 17.957 $m^2 g^{-1}$ for the addition amount of 2, 3, 4, and 5 g TBT, respectively. As a result, the C-doped hollow TiO_2 spheres with a shell thickness that varies from 20 to 59 nm can be easily controlled by tailoring the addition amount of TBT. In most cases, the hollow TiO_2 spheres with high shell thickness are beneficial to hinder the form of fragile spheres and improve the mechanical stability and adsorption properties of the spheres [35,36].

3.3. Crystal structure and bonding environment of C-doped hollow TiO_2 spheres

The XRD analysis was used to characterize the phase structures of the synthesized C-doped hollow TiO_2 spheres. Fig. 4 shows that all the reflection peaks appeared at $2\theta = 25.4°$ (101), 37.9° (004), 48.0° (200), 53.8° (105), 54.9° (211) and 62.8° (204) are able to be indexed to the anatase of TiO_2 (JCPDS: No 21-1272) [5,37]. The diffraction peaks of the hollow C-doped TiO_2 spheres are sharp and intense, indicating the highly crystalline character of the prepared hollow TiO_2 [5]. The crystallite particle size is calculated by using the Scherrer analysis of the different XRD profiles (Fig. 4). Crystalline particle size is about 15.2, 9.1,10.3, and 12.5 nm for the addition amount of TBT 2, 3, 4, and 5 g, respectively.

The existence of the carbon element in the hollow TiO_2 spheres is proved by elemental analysis (EA) and X-ray photoelectron spectroscopy (XPS). Its content approaches to 1.985 wt% according to the EA analysis. More detailed information considering the chemical and bonding environment of the TiO_2 matrix and carbon phase

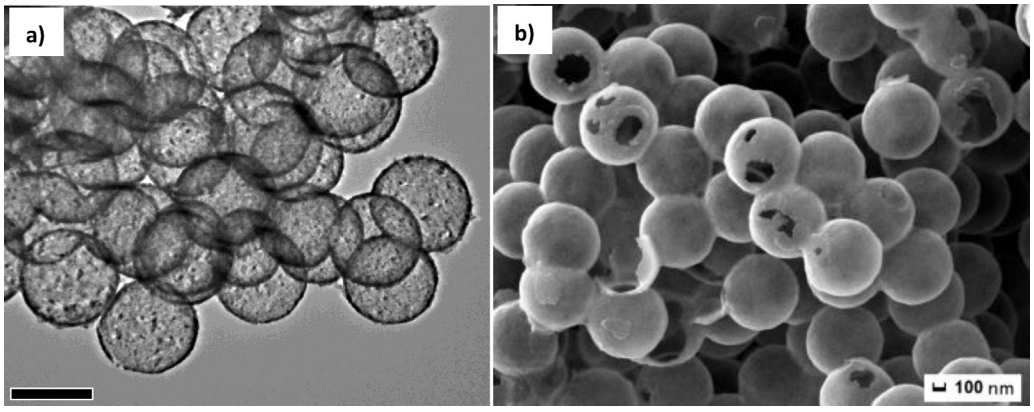

Fig. 1. TEM and SEM images of hollow TiO_2 spheres.

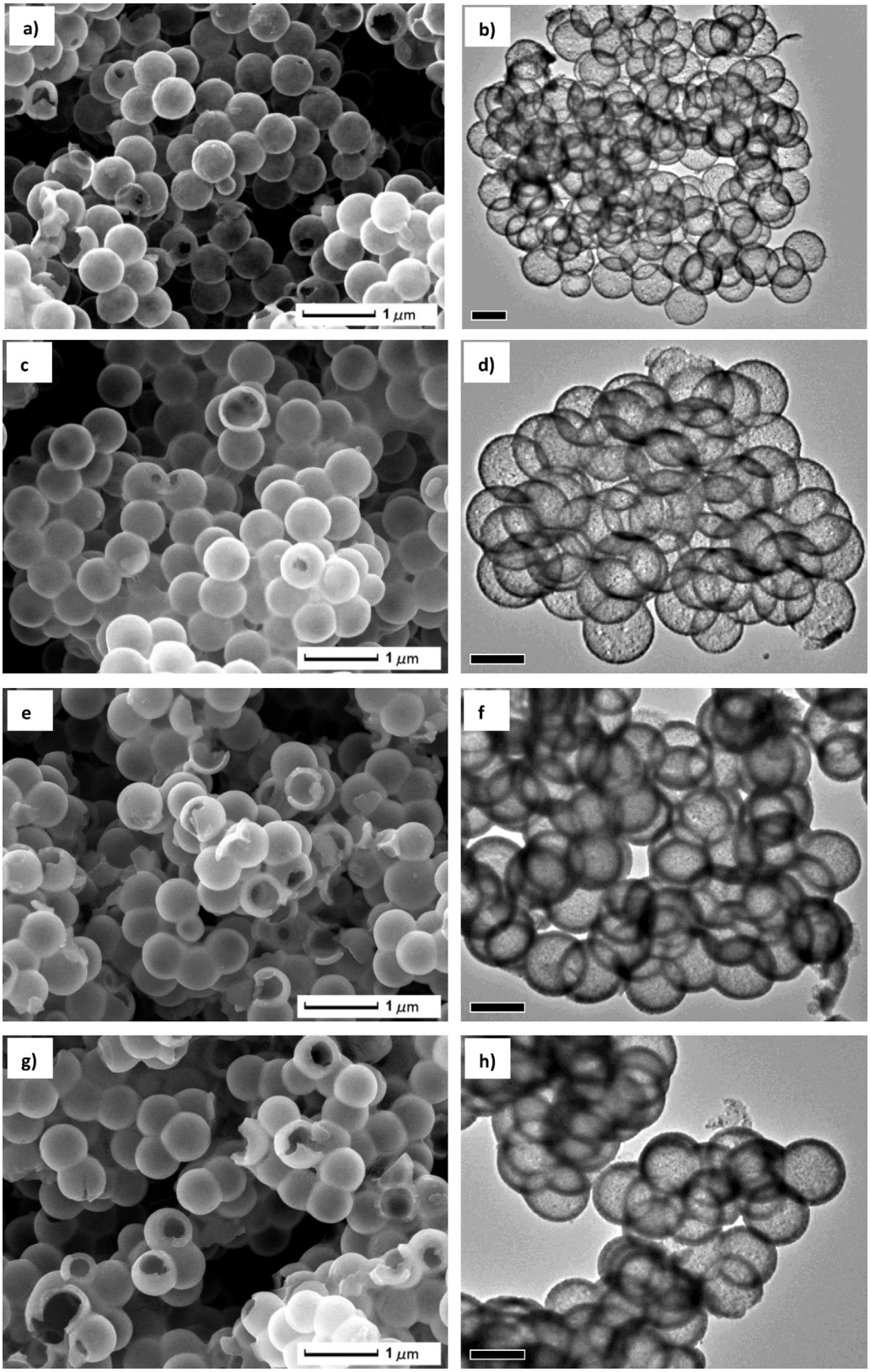

Fig. 2. SEM and TEM images of the C-doped hollow TiO_2 spheres produced with different amount of TBT added. (a, b) 2 g; (c, d) 3 g; (e, f) 4 g, and (g, h) 5 g.

is ascertained using XPS [5,11,38]. Fig. 5a shows that the elements of C, Ti, and O can be clearly identified with the binding energies of C 1s, Ti 2p, and O 1s electrons, suggesting that the prepared hollow TiO_2 spheres contain carbon (the carbon signals in hollow TiO_2 spheres are responsible for the cationic polystyrene templates used to prepare the hollow TiO_2 spheres) and TiO_2 [13]. For the Ti 2p high-resolution XPS spectra, as demonstrated in Fig. 5b, the peak located at 464.23 eV corresponds to the Ti $2p_{1/2}$ and another one

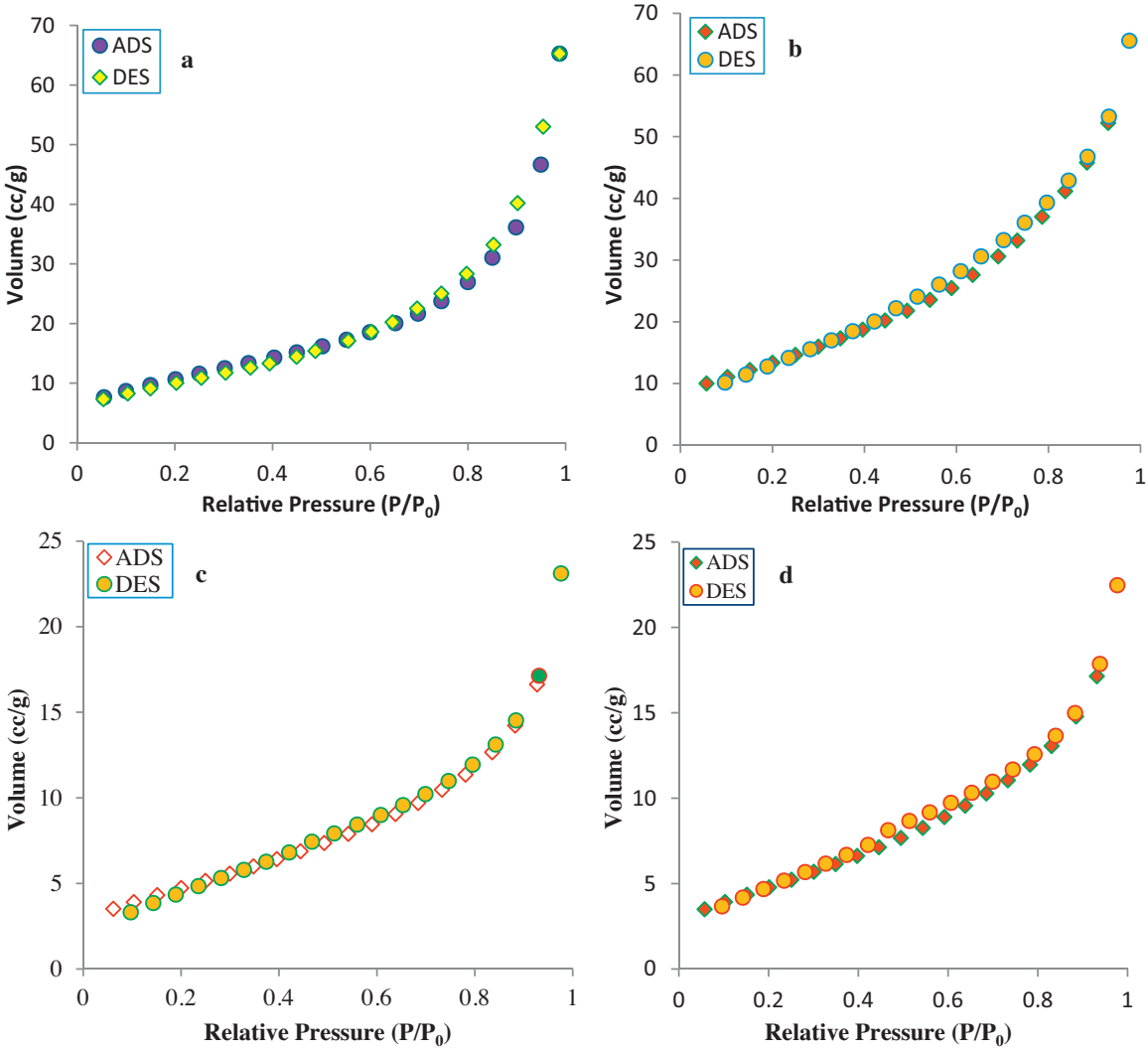

Fig. 3. N_2 adsorption/desorption isotherms of C-doped hollow TiO_2 spheres prepared with different amount of TBT added. (a) 2 g; (b) 3 g; (c) 4 g, and (d) 5 g.

located at 458.55 eV is assigned to Ti $2p_{3/2}$. The splitting between Ti $2p_{1/2}$ and Ti $2p_{3/2}$ is 5.68 eV, indicating a normal state of Ti^{4+} in the C-doped TiO_2 hollow spheres [5,11]. Moreover, The Ti $2p_{3/2}$ binding energy for the C-doped hollow TiO_2 spheres is 458.49 eV, an increase of 0.25 eV. The Ti $2p_{1/2}$ binding energy for the undoped P25 (Degussa) sample is 464.0 eV in literature [39], again an increase of 0.23 eV. In both cases, the binding energy increases upon C-doping, strongly indicating lattice distortions [39].

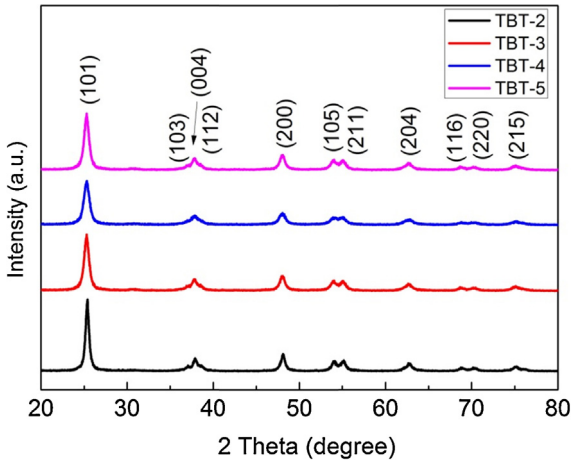

Fig. 4. XRD patterns of C-doped hollow TiO_2 spheres (samples in Figs. 2 and 3).

Fig. 5c indicates that the main C 1s peak is dominated by elemental carbon at 284.67 eV, attributed mainly to extensively delocalized alternant hydrocarbon, the two peaks at 286.3 and 288.56 eV are characteristic of the oxygen bound species C–O and Ti-O-C, respectively [37,39]. Excitedly, C1s characteristic peak at 280.65 eV is observed and has been related to Ti–C or carbon substitutionally doped in the place of oxygen in the TiO_2 lattice [23,40,41], strongly suggesting that the existence of C-doping from the binding energies of the electrons relates to C 1s. Therefore, multiple carbon species, namely substitutional and interstitial carbon atoms and carbonate species, exist in the lattice of the as-prepared hollow TiO_2 spheres [42]. On the other hand, compared with the O1s binding energies of undoped P25 (Degussa), The O1s binding energies for the C-doped samples (Fig. 5d) also displays a clear shift. This is from 529.6 eV obtained from a previous publication [39] in the undoped TiO_2 materials to 529.99 eV in the C-doped hollow TiO_2 sample and from 530.9 eV in the undoped to 532.04 eV in the doped sample, again indicating lattice distortion upon doping [39].

UV–vis diffuse reflectance spectroscopy was further used to measure the electronic states of the as-synthesized C–TiO_2 samples

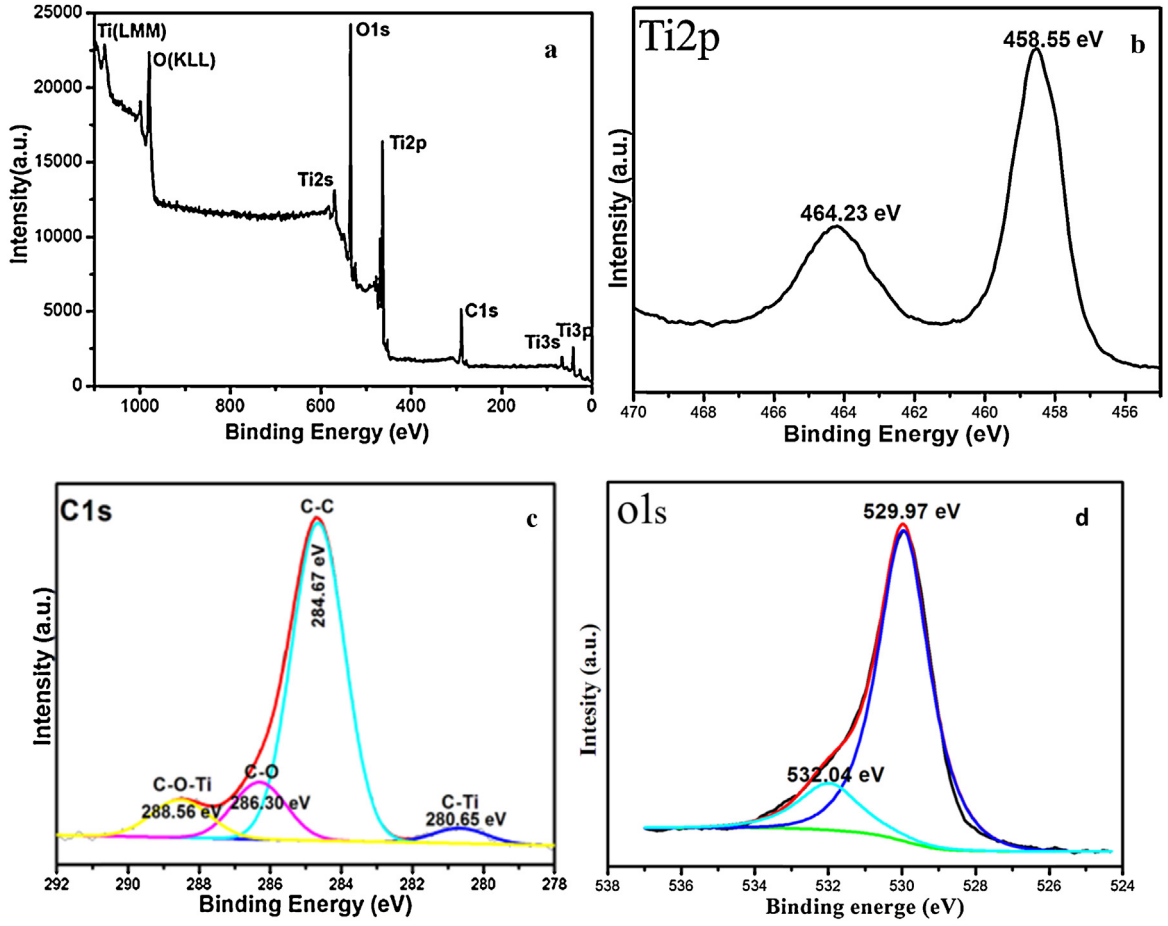

Fig. 5. (a) XPS fully scanned spectra of the C-doped hollow TiO_2 sample; (b) XPS spectra of Ti 2p; (c) XPS spectrum of C 1s and (d) XPS spectra of O 1s for the C-doped hollow TiO_2 samples.

using the spectrum of Degussa P25 TiO_2 as a reference profile. Fig. 6 indicates that there is no any adsorption for P25 over their fundamental absorption band edge at about 410 nm. Significant red-shift (red curve) in the UV–vis absorption spectra is observed for carbon-doped hollow TiO_2 spheres thanks to the photo absorption property of the carbonaceous species in the as-synthesized TiO_2 composites [37]. Similar red-shift for carbon-doped TiO_2 has been also confirmed by previous investigators [37,39].

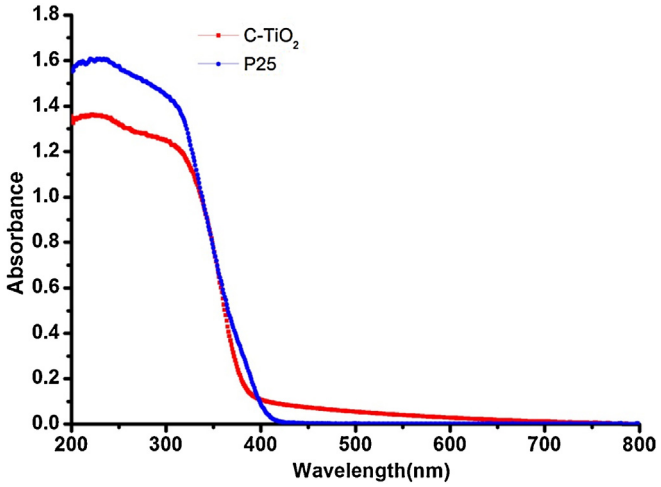

Fig. 6. UV–vis absorbance spectra of undoped P25 and prepared C–TiO_2 samples.

3.4. Photocatalytic activity of C-doped hollow TiO_2 spheres

TiO_2-based materials can manifest superior performances in many important applications such as dye-sensitized solar cells and photocatalysis. Here, we demonstrate the potential applicability of the C-doped hollow TiO_2 spheres as an excellent photocatalyst for the degradation of Rhodamine B (RhB) under visible-light irradiation, where commercial P25 TiO_2 is usually used as a reference photocatalyst [27,39,42]. As shown in Fig. 7a, with increasing illumination time, the characteristic absorption band of the dye (about 553 nm) [25,28] vanishes gradually and completely disappears after about 40 mins during visible-light irradiation. Compared with the undoped P25 (Degussa) TiO_2 (Fig. 7b), interestingly, the characteristic absorption band of the RhB exhibits a more markedly blue shift (from 553 to 495 nm). The gradual hypsochromic shifts of the absorption maximum result from the *N*-deethylation of RhB during irradiation. This hypsochromic shift corresponds to a step-by-step deethylation of RhB to produce *N*,*N*,*N*′-triethyl rhodamine (TER, 539 nm), *N*,*N*′-diethyl rhodamine (DER, 522 nm), *N*-ethylrhodamine (MER, 510 nm), and rhodamine at 498 nm [43]. In order to explain the increased visible-light activity of C-doped TiO_2, a possible mechanism is proposed. With the substitution for oxygen atoms by carbon atoms in the crystal lattice of TiO_2, new impurity is introduced between the conduction and valence band of TiO_2, then the electrons are able to be promoted to the conduction band from the impurity level, producing a narrower band gap than Degussa P25 TiO_2 and the absorption in the visible-light region [7,42].

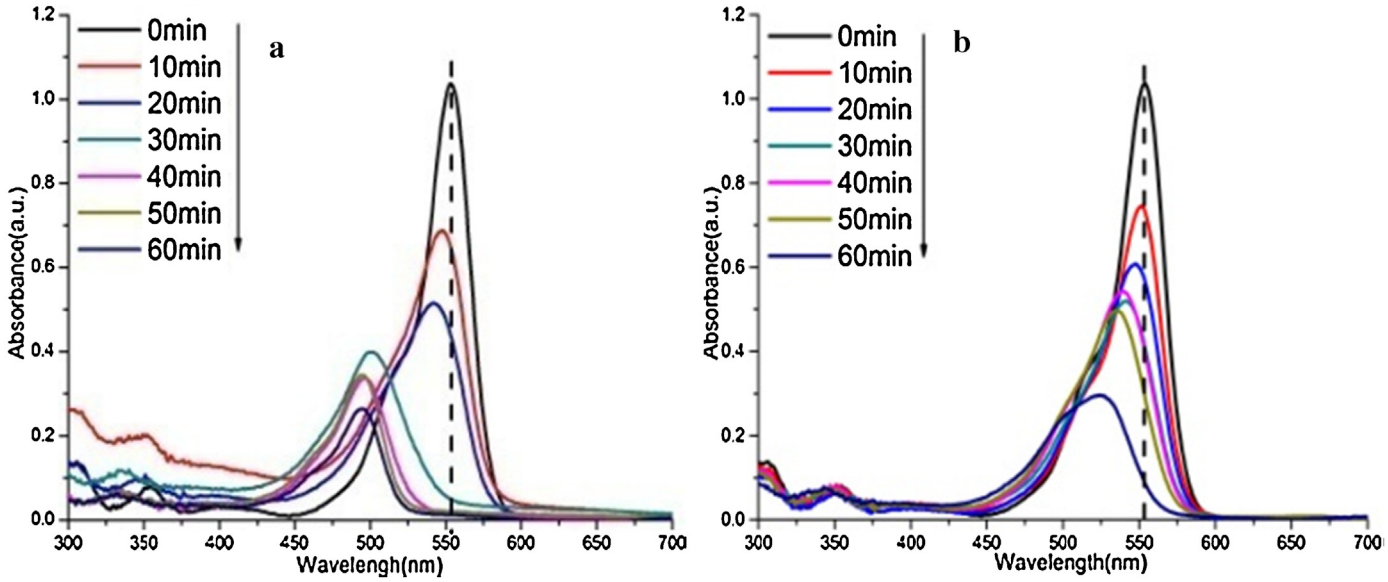

Fig. 7. UV–vis spectra of the aqueous solutions of RhB dye over C-doped hollow TiO_2 spheres (a) and P25 (b).

Time course of the decrease in the dye concentration using two catalysts was shown in Fig. 8. Under the visible-light irradiation in a short period of 20 mins, the C-doped samples are able to degrade about 56% of the original organic RhB dye, while value for the Degussa P25 is only about 44%. Excitedly, after visible-light irradiation 30 min, RhB is degraded by 95%, completely degraded under the irradiation of visible light for 40 mins far over the value (~60%) for undoped P25. Unexpectedly, the C-doped hollow TiO_2 spheres produced in this work manifest the superior photocatalytic activity over the photocatalytic efficiencies of most of TiO_2-based photocatalysts reported in literature (e.g. hollow TiO_2, porous TiO_2@C microspheres, fluorinated B/C-Co-doped TiO_2 nanocrystals, and Fe_3O_4@C@F-TiO_2 microspheres) [23–27]. Fig. 8b shows the degradation versus time profiles for the photocatalytic oxidation of RhB under visible light using TOC analysis. It is clear that C-doped hollow TiO_2 spheres manifest better photocatalytic ability than Degussa P25 TiO_2, which fairly agrees with the results measured by UV–vis spectrum. Clearly, carbon doped in the place of oxygen in the TiO_2 lattice plays an optical absorption role in extending the response of hollow TiO_2 spheres into the visible light range of the solar spectrum [5,37].

3.5. *Effect of shell thickness on photocatalytic activity*

Tuning the shell thickness of C-doped hollow TiO_2 spheres, in this work, is so easy only through changing the addition amount of TBT. To achieve the greatest photocatalytic activity, the optimal shell thickness needs to be investigated. Fig. 9 shows that the as-synthesized C-TiO_2 spheres both exhibit better photocatalytic ability than Degussa P25 TiO_2 with the highest BET surface area (Fig. S5, ~58.402 $m^2\,g^{-1}$) and demonstrates that a uniform shell thickness (TBT-2 g, ~20 nm) is preferable in degrading RhB in comparison to C-TiO_2 spheres with ill-defined morphology and size (TBT-1g, broken spheres). When shell thickness is increased to ~29 nm (TBT-3g), the highest photocatalytic ability is observed due to its higher surface area (50.270 $m^2\,g^{-1}$) and C content (2.795%) determined by elemental analysis. When the thickness is further increased to ~59 nm (TBT-5g), the lowest degradation of RhB is

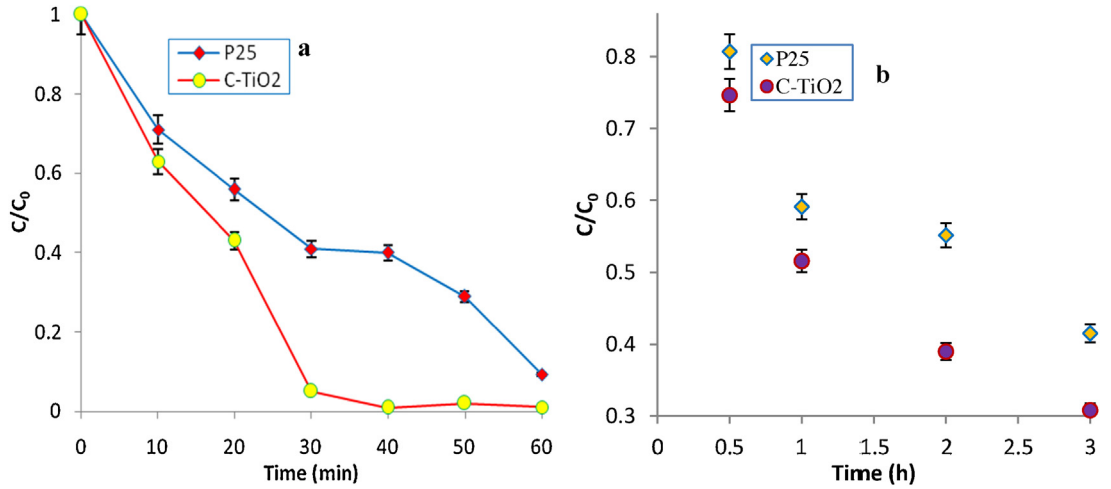

Fig. 8. Changes in the concentration of dye RhB during the photocatalytic reaction in the presence of P25 and C-doped hollow TiO_2 spheres under visible-light irradiation: (a) UV analysis; (b) TOC analysis.

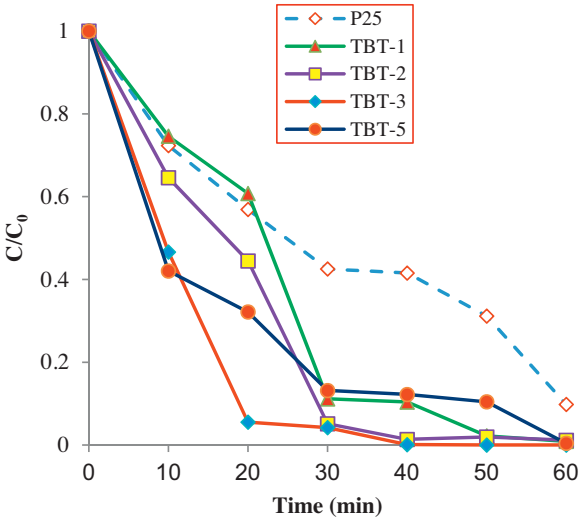

Fig. 9. Changes in the concentration of dye RhB during the photocatalytic reaction (samples in Figs. 2 and 3).

obtained because of its decreased surface area (~17.957 $m^2 g^{-1}$), although its C content approaches 4.435%. This indicates that a uniform, optimal shell thickness is of practical use for C-TiO_2 hollow spheres because it offers more space and active sites for the adsorption of RhB.

4. Conclusions

In summary, we have devised an *in situ* synthetic method to create C-doped hollow spheres by using cationic polystyrene spheres as templates. The as-prepared TiO_2 spheres offer a well-defined size that is determined by the diameter of the CPS template and a homogeneous shell whose thickness is readily controlled only through changing the addition amount of TBT. Excitedly, under the removal of CPS templates by calcination at 450 °C, carbon element is doped in the place of oxygen in the TiO_2 lattice, *in situ* forming C-doped hollow anatase TiO_2 spheres. When used as photocatalysts for the degradation of RhB under visible-light irradiation, As-created C-doped hollow TiO_2 spheres manifest a superior photocatalytic ability over commercial P25 and many TiO_2-based photocatalysts, considerably broadening potential for many practical applications. Therefore, this work provides a facile and cost-effective protocol to the *in situ* synthesis of the C-doped hollow TiO_2 spheres with controlled architectures, which is beneficial to shift the ultraviolet to visible-light-driven photocatalysis.

Acknowledgements

The authors would like to thank Jiangsu Natural Science Fund of China (No. BK20141299) and National Natural Science Foundation of China (No. 21163008) for financial support to carry out this work.

Appendix A. Supplementary data

Supplementary data associated with this article can be found, in the online version, at http://dx.doi.org/10.1016/j.apcatb.2014.10.063.

References

[1] M. Setvín, U. Aschauer, P. Scheiber, Y. Li, W. Hou, M. Schmid, A. Selloni, U. Diebold, Science 341 (2013) 988.
[2] T. Fröschl, U. Hörmann, P. Kubiak, G. Kučerová, M. Pfanzelt, C. Weiss, R. Behm, N. Hüsing, U. Kaiser, K. Landfester, M. Wohlfahrt-Mehrens, Chem. Soc. Rev. 41 (2012) 5313.
[3] L. Jing, W. Zhou, G. Tian, H. Fu, Chem. Soc. Rev. 42 (2013) 9509.
[4] C. Lin, Y. Song, L. Cao, S. Chen, J. Chin. Adv. Mater. Soc. 1 (2013) 188.
[5] P. Zhang, C. Shao, Z. Zhang, M. Zhang, J. Mu, Z. Guo, Y. Liu, Nanoscale 3 (2011) 2943.
[6] L. Zhang, M. Tse, O. Tan, Y. Wang, M. Han, J. Mater. Chem. A 1 (2013) 4497.
[7] C. Valentin, G. Pacchioni, A. Selloni, Chem. Mater. 17 (2005) 6656.
[8] K. Woan, G. Pyrgiotakis, W. Sigmund, Adv. Mater. 21 (2009) 2233.
[9] G. Zhang, F. Teng, Y. Wang, P. Zhang, C. Gong, L. Chen, C. Zhao, E. Xie, RSC Adv. 3 (2013) 24644.
[10] A. Kongkanand, P.V. Kamat, ACS Nano 1 (2007) 13.
[11] S. Lee, Y. Lee, D.H. Kim, J. Moon, ACS Appl. Mater. Interf. 5 (2013) 12526.
[12] Z. He, W. Que, Y. He, RSC Adv. 4 (2014) 3332.
[13] L. Li, Y. Zhu, X. Lu, M. Wei, W. Zhuang, Z. Yang, X. Feng, Chem. Commun. 48 (2012) 11525.
[14] S. Khan, M. Al-Shahry, W.B. Ingler, Science 297 (2002) 2243.
[15] V. Kiran, S. Sampath, Nanoscale 5 (2013) 10646.
[16] L. Quan, Y. Jang, K. Stoerzinger, K. May, Y. Jang, S. Kochuveedu, Y.S. Horn, D.H. Kim, Phys. Chem. Chem. Phys. 16 (2014) 9023.
[17] M. Murdoch, G. Waterhouse, M. Nadeem, J. Metson, M. Keane, R. Howe, J. Llorca, H. Idriss, Nat. Chem. 3 (2011) 489.
[18] J. Zhou, L. Lv, J. Yu, H. Li, P. Guo, H. Sun, X. Zhao, J. Phys. Chem. C 112 (2008) 5316.
[19] Y. Yu, X. Yin, A. Kvit, X. Wang, Nano Lett. 14 (2014) 2528.
[20] J. Yu, J. Zhang, Dalton Trans. 39 (2010) 5860.
[21] Z. Jin, F. Wang, F. Wang, J. Wang, J. Yu, J. Wang, Adv. Funct. Mater. 23 (2013) 2137.
[22] J. Joo, M. Dahl, N. Li, F. Zaera, Y. Yin, Energy Environ. Sci. 6 (2013) 2082.
[23] J. Yu, Q. Li, S. Liu, M. Jaroniec, Chem. Eur. J. 19 (2013) 2433.
[24] J. Zhuang, Q. Tian, H. Zhou, Q. Liu, P. Liu, H. Zhong, J. Mater. Chem. 22 (2012) 7036.
[25] W. Zhao, L. Feng, R. Yang, J. Zheng, X. Li, Appl. Catal. B: Environ. 103 (2011) 181.
[26] D. Li, Q. Qin, X. Duan, J. Yang, W. Guo, W. Zheng, ACS Appl. Mater. Interf. 5 (2013) 9095.
[27] G. Liu, F. He, J. Zhang, L. Li, F. Li, L. Chen, Y. Huang, Appl. Catal. B: Environ. 150–151 (2014) 515.
[28] H. Wu, H. Hng, X. Lou, Adv. Mater. 24 (2012) 2567.
[29] S. Cao, J. Chen, Y. Ge, L. Fang, Y. Zhang, A.P.F. Turner, Chem. Commun. 50 (2014) 118.
[30] S. Cao, L. Fang, Z. Zhao, Y. Ge, S. Piletsky, A.P.F. Turner, Adv. Funct. Mater. 23 (2013) 2162.
[31] K. Qi, X. Chen, Y. Liu, J. Xin, C. Mak, W. Daoud, J. Mater. Chem. 17 (2007) 3504.
[32] X. Lü, F. Huang, X. Mou, Y. Wang, F. Xu, Adv. Mater. 22 (2010) 3719.
[33] T. Leshuk, S. Linley, G. Baxter, F. Gu, ACS Appl. Mater. Interf. 4 (2012) 6062.
[34] S. Liu, J. Yu, M. Jaroniec, J. Am. Chem. Soc. 132 (2010) 11914.
[35] H.G. Bagaria, S.B. Kadali, M.S. Wong, Chem. Mater. 23 (2011) 301.
[36] Z. Li, B. Gao, G.Z. Chen, R. Mokaya, S. Sotiropoulos, G.L. Puma, Appl. Catal. B: Environ. 110 (2011) 50.
[37] B. Li, Z. Zhao, F. Gao, X. Wang, J. Qiu, Appl. Catal. B: Environ. 147 (2014) 958.
[38] C. Lin, Y. Song, L. Cao, S. Chen, Nanoscale 5 (2013) 4986.
[39] E.M. Neville, M.J. Mattle, D. Loughrey, B. Rajesh, M. Rahman, J.M. Don MacElroy, J.A. Sullivan, K.R. Thampi, J. Phys. Chem. C 116 (2012) 16511.
[40] V. Etacheri, G. Michlits, M.K. Seery, S.J. Hinder, S.C. Pillai, ACS Appl. Mater. Interf. 5 (2013) 1663.
[41] S. In, A. Kean, A. Orlov, M. Tikhov, R. Lambert, Energ. Environ. Sci. 2 (2009) 1277.
[42] X. Yang, C. Cao, L. Erickson, K. Hohn, R. Maghirang, K. Klabunde, Appl. Catal. B: Environ. 91 (2009) 657.
[43] H. Fu, S. Zhang, T. Xu, J. Chen, Environ. Sci. Technol. 42 (2008) 2085.

Update

Applied Catalysis B: Environmental
Volume 166–167, Issue , May 2015, Page 644

DOI: https://doi.org/10.1016/j.apcatb.2014.11.054

Applied Catalysis B: Environmental 166–167 (2015) 644

Contents lists available at ScienceDirect

Applied Catalysis B: Environmental

journal homepage: www.elsevier.com/locate/apcatb

Corrigendum

Corrigendum to "C-doped hollow TiO_2 spheres: In situ synthesis, controlled shell thickness, and superior visible-light photocatalytic activity" [Appl. Catal. B: Environ. 165 (2015) 715–722]

Ying Zhang[a], Zhiyuan Zhao[a], Juanrong Chen[b], Li Cheng[a], Jun Chang[a], Weichen Sheng[a], Changyuan Hu[c], Shunsheng Cao[a,*]

[a] School of Materials Science and Engineering, Jiangsu University, Zhenjiang 212013, PR China
[b] School of Environment and Safety Engineering, Jiangsu University, Zhenjiang 212013, PR China
[c] Jiangxi Key Laboratory of Surface Engineering, Jiangxi Science and Technology Normal University, Nanchang 330013, PR China

The authors regret to inform that affiliation 'a' was published incorrectly. The correct affiliation is "School of Materials Science and Engineering, Jiangsu University, Xuefu Road 301, Zhenjiang 212013, PR China".

Author would like to apologize for the inconvenience caused.

DOI of original article: http://dx.doi.org/10.1016/j.apcatb.2014.10.063.
* Corresponding author.
E-mail addresses: sscaochem@hotmail.com, sscao@ujs.edu.cn (S. Cao).

http://dx.doi.org/10.1016/j.apcatb.2014.11.054